2009 American Control Conference
Hyatt Regency Riverfront, St. Louis, MO, USA
June 10-12, 2009

Stability Analysis of Central Difference Method for Dynamic Real-time Substructure Testing

B. Wu, L. Deng, Z. Wang, and X. Yang

Abstract—**This paper studies the stability of the central difference method (CDM) for real-time substructure test considering the mass of specimen (i.e., experimental substructure). To obtain correct reaction inertia force, an explicit acceleration formulation is assumed for the CDM. The analytical work shows that the stability of the algorithm decreases with increasing specimen mass if the experimental substructure is a pure inertia specimen. The algorithm becomes unstable whatever the time integration interval, i.e., unconditionally unstable, when the mass of specimen equal or greater than that of its numerical counterpart. For the case of dynamic specimen, the algorithm is unconditionally unstable when there is no damping in the whole test structure; a damping will make the algorithm stable conditionally. The behavior of the CDM for vanishing time integration interval is verified with the zero-stability analysis method for coupled integration. Part of the analytical results is validated by an actual test.**

I. INTRODUCTION

REAL-time substructure testing (RSTing) is a hybrid simulation technique, in which a structure is split into two parts: the critical complex part called experimental substructure to be tested physically and in real-time, while the remainder called numerical substructure is simulated numerically by the computer [1]. As a core element of the analytical part of RSTing, numerical integration plays a key role in a successful test. Many integration methods popular in PDT are explicit only for displacement. When an explicit velocity is required for damping specimen (experimental substructure) in RSTs, some extra formulation has to be assumed. This assumption very possibly does not conform to the original velocity formulation and this may change the numerical behavior of the integration algorithm. For the central difference method (CDM) in RSTing with damping specimen, reference [2] showed that the stability decreases with increasing damping of the experimental substructure, contrasting constant stability limit of standard CDM. Similar problem may exist for implicit algorithm implemented in a RST. Reference [3] found that Newmark average acceleration method may lose the unconditional stability for damping specimen.

For a dynamic experimental substructure, the loading fashion should be explicitly and properly specified to obtain correct reaction of the substructures due to its inertia as well as stiffness and damping. This may change the numerical behavior of integration algorithms which normally do not include any explicit expressions for acceleration. Reference [4] showed that the Newmark average acceleration method became conditionally stable when the loading commands for the dynamic substructure were sent off as a linear ramp function of time. Although here have been successful applications of explicit algorithms to inertia specimen and some discussions on stability related to time delay [5] or coupling between numerical and experimental substructures [6], the impact of specimen mass on the stability of a specific integration method has not been explored. This paper will focus on the stability issue of the CDM arising in its implementation to RSTing with dynamic experimental substructure.

II. FORMULATION OF THE CDM FOR RST CONSIDERIING SPECIMEN MASS

In an RST, the acceleration-dependent force (inertia force) and velocity-dependent force (damping force) exhibited by the specimen are introduced into the measured reaction force together with the static restoring force when the specimen is a dynamic substructure. Therefore, the time-discretized equations of motion of the numerical substructure at the *i*th time step in an RST can be expressed in a more general and precise form as

$$\boldsymbol{M}_{\mathrm{N}}\,\boldsymbol{a}_{\mathrm{N},i}+\boldsymbol{C}_{\mathrm{N}}\,\boldsymbol{v}_{\mathrm{N},i}+\boldsymbol{K}_{\mathrm{N}}\,\boldsymbol{d}_{\mathrm{N},i}+\boldsymbol{R}_{\mathrm{E}}(\boldsymbol{a}_{\mathrm{EC},i},\boldsymbol{v}_{\mathrm{EC},i},\boldsymbol{d}_{\mathrm{EC},i})=\boldsymbol{F}_{i} \qquad (1)$$

and, when the CDM is employed, the velocity and acceleration are approximated by

$$\boldsymbol{v}_{\mathrm{N},i}=(\boldsymbol{d}_{\mathrm{N},i+1}-\boldsymbol{d}_{\mathrm{N},i-1})/2\Delta t \qquad (2)$$

$$\boldsymbol{a}_{\mathrm{N},i}=(\boldsymbol{d}_{\mathrm{N},i+1}-2\boldsymbol{d}_{\mathrm{N},i}+\boldsymbol{d}_{\mathrm{N},i-1})/\Delta t^{2} \qquad (3)$$

where $\boldsymbol{M}$, $\boldsymbol{C}$, and $\boldsymbol{K}$ are the mass, damper, and stiffness matrices of the numerical substructure respectively; $\boldsymbol{R}$ is the reaction force; $\boldsymbol{a}$, $\boldsymbol{v}$, and $\boldsymbol{d}$ are acceleration, velocity, and displacement vectors; $\boldsymbol{F}$ is external excitation on the

This work was supported by Grant 90715036 and 50578047 from the National Science Foundation of China, and China Ministry of Education through Program for New Century Excellent Talents in University.

B. Wu is with the School of Civil Engineering, Harbin Institute of Technology, HARBIN 150090 CHINA (e-mail: bin.wu@hit.edu.cn).

L. Deng and Z. Wang are with the School of Civil Engineering, Harbin Institute of Technology, HARBIN 150090 CHINA.

X. Yang is with China Southwest Architectural Design and Research Institute, CHENGDU 610081 CHINA (e-mail: yangxd_tom@163.com).

numerical substructure; Δt is the integration time interval; subscripts N, E, and C denote numerical substructure, experimental substructure, and coupling degree-of-freedom of numerical and experimental substructures, respectively. Substituting (2) and(3) into (1) gives

$$\begin{aligned}\boldsymbol{d}_{\mathrm{N},i+1} = &[\boldsymbol{M}_{\mathrm{N}}/\Delta t^2 + \boldsymbol{C}_{\mathrm{N}}/(2\Delta t)]^{-1} \\ &\cdot\{\boldsymbol{F}_i - (\boldsymbol{K}_{\mathrm{N}} - 2\boldsymbol{M}_{\mathrm{N}}/\Delta t^2)\boldsymbol{d}_{\mathrm{N},i} - [\boldsymbol{M}_{\mathrm{N}}/\Delta t^2 \\ &- \boldsymbol{C}_{\mathrm{N}}/(2\Delta t)]\boldsymbol{d}_{\mathrm{N},i-1} - \boldsymbol{R}_{\mathrm{E}}(\boldsymbol{a}_{\mathrm{EC},i}, \boldsymbol{v}_{\mathrm{EC},i}, \boldsymbol{d}_{\mathrm{EC},i})\}\end{aligned} \tag{4}$$

To obtain accurate dynamic reaction force, the velocity and acceleration on the coupling degree-of-freedom at the (i+1)th step, which denoted by $\boldsymbol{v}_{\mathrm{EC},i+1}$ and $\boldsymbol{a}_{\mathrm{EC},i+1}$ respectively, have to be determined and imposed onto the specimen together with $\boldsymbol{d}_{\mathrm{EC},i+1}$. This just can not be realized through (2) and (3), as the displacement at the (i+2)th step is not yet available. For an actuator controlled in a traditional displacement mode, the achievement of the explicit velocity or acceleration target is dependent on how the displacement command is issued with respect with time. To this end, we assume a constant acceleration in the time interval from t_{i} to $t_{\mathrm{i+1}}$, resulted in by a displacement command profile as a quadratic function in time:

$$\boldsymbol{d}_{\mathrm{EC},i+1}(t) = \boldsymbol{d}_{\mathrm{EC},i} + \boldsymbol{v}_{\mathrm{EC},i}(t - t_i) + 0.5\boldsymbol{a}_{\mathrm{EC},i+1}(t - t_i)^2 \tag{5}$$

Note that, for seismic tests, the commands should include the ground motion to guarantee an absolute acceleration input to the dynamic specimen and hence obtain correctly reaction force due to inertia. Letting $\boldsymbol{d}_{\mathrm{EC},i}$=$\boldsymbol{d}_{\mathrm{NC},i}$ and $\boldsymbol{v}_{\mathrm{EC},i}$=$\boldsymbol{v}_{\mathrm{NC},i}$, and substituting (2) into the above equation and letting t=t_{i+1} entail

$$\boldsymbol{a}_{\mathrm{EC},i+1} = (\boldsymbol{d}_{\mathrm{NC},i+1} - 2\boldsymbol{d}_{\mathrm{NC},i} + \boldsymbol{d}_{\mathrm{NC},i-1})/\Delta t^2 \tag{6}$$

It is interesting to note that

$$\boldsymbol{a}_{\mathrm{EC},i+1} = \boldsymbol{a}_{\mathrm{NC},i} \tag{7}$$

according to (3).

By comparing (6) with (3), we see that the acceleration at the coupling degree-of freedom of the experimental substructure is obviously no longer consistent to those of numerical substructure determined by the standard CDM. This raises the issue of possible change of numerical behavior, especially the stability, of the modified CDM over the standard one, which will be discussed next.

III. STABILITY ANALYSIS

We restrain our discussion within linear systems and the numerical substructure is of single-degree-of-freedom (SDOF). Two cases are considered: one is with a specimen of pure mass as shown Fig. 1, and the other with a SDOF dynamic specimen as shown Fig. 2.

A. Pure Inertia Specimen

When the experimental substructure is just an inertia specimen, its reaction force at the ith step is easily obtained as

$$R_{\mathrm{E},i} = M_{\mathrm{E}}\, a_{\mathrm{EC},i} \tag{8}$$

where $a_{\mathrm{EC},i}$ is determined by (6) . Substituting (8) into (4) yields

$$\begin{aligned}d_{i+1} = &[M_{\mathrm{N}}/\Delta t^2 + C_{\mathrm{N}}/(2\Delta t)]^{-1} \\ &\cdot\{F_i - [K_{\mathrm{N}} - (2M_{\mathrm{N}} - M_{\mathrm{E}})/\Delta t^2]\, d_i \\ &- [(M_{\mathrm{N}} - 2M_{\mathrm{E}})/\Delta t^2 - C_{\mathrm{N}}/(2\Delta t)]\, d_{i-1} \\ &- M_{\mathrm{E}}/\Delta t^2\, d_{i-2}\}\end{aligned} \tag{9}$$

Based on the above equation, the displacement responses of free vibration between two adjacent time steps can be related in a recursive form as

$$\boldsymbol{Y}_{i+1} = \boldsymbol{A}\boldsymbol{Y}_i \tag{10}$$

where $\boldsymbol{Y}_{i+1} = \begin{bmatrix} d_{i+1} & d_i & d_{i-1}\end{bmatrix}^{\mathrm{T}}$, $\boldsymbol{A} = \begin{bmatrix} a_{11} & a_{12} & a_{13} \\ 1 & 0 & 0 \\ 0 & 1 & 0\end{bmatrix}$ with $a_{11} = [2 - (1+\gamma_{\mathrm{m}})\,\Omega^2 - \gamma_{\mathrm{m}}]/(1+\xi_{\mathrm{N}}\,\Omega)$, $a_{12} = (\xi_{\mathrm{N}}\,\Omega + 2\gamma_{\mathrm{m}} - 1)/(1+\xi_{\mathrm{N}}\,\Omega)$, $a_{13} = -\gamma_{\mathrm{m}}/(1+\xi_{\mathrm{N}}\,\Omega)$, $\Omega = \Delta t\,\omega = \Delta t\sqrt{K_{\mathrm{N}}/(M_{\mathrm{N}} + M_{\mathrm{E}})}$, $\xi_{\mathrm{N}} = C_{\mathrm{N}}/(2M_{\mathrm{N}}\,\omega)$, γ_{m}=M_{E}/M_{N}. The matrix $\boldsymbol{A}$ is usually called amplification matrix and its eigenvalues determine the numerical behavior of an integration algorithm. In particular, the amplification matrix defines the stability condition of an integration algorithm through

$$\rho(\boldsymbol{A}) \le 1 \tag{11}$$

where $\rho(\boldsymbol{A})$ is the spectral radius of $\boldsymbol{A}$, which is defined as ρ ($\boldsymbol{A}$) =max($|\lambda_{\mathrm{i}}|$), andλ_{i} are the eigenvalues of $\boldsymbol{A}$. The characteristic equation of $\boldsymbol{A}$ can be obtained as

$$\begin{aligned}(1+\xi_{\mathrm{N}}\,\Omega)\,\lambda^3 + &\left[(1+\gamma_{\mathrm{m}})\,\Omega^2 - 2 + \gamma_{\mathrm{m}}\right]\lambda^2 \\ &+ (1 - \xi_{\mathrm{N}}\,\Omega - 2\gamma_{\mathrm{m}})\,\lambda + \gamma_{\mathrm{m}} = 0\end{aligned} \tag{12}$$

We define a stability limit as the maximum of the Ω_{s} values such that $\rho(\boldsymbol{A})\le 1$ for any $\Omega\in(0, \Omega_{\mathrm{s}})$. Letting $[\Omega]$ denote the stability limit, one may obtain the stability limit of the modified CDM for pure inertia specimen as [7]

$$[\Omega] = 2\sqrt{(1-\gamma_m)/(1+\gamma_m)} \quad (13)$$

The above equation indicates that (i) the stability limit only exists when $\gamma_m<1$ (the non-existence of stability limit is called unconditionally unstable in this paper); (ii) the stability limit decreases with increasing γ_m; and (iii) the stability limit has no relationship with damping from numerical substructure. The interesting behavior of unconditional instability can also be proved through the concept of zero-stability of coupled integration. The proof is provided in the appendix.

The spectral radius $\rho(\boldsymbol{A})$ against Ω is plotted in Fig. 3a with $\xi_N=0$ and different γ_m values. The stability limits obtained from Fig. 3a are identical to those calculated using (13). Fig. 3b shows the diagrams of spectral radius $\rho(\boldsymbol{A})$ against Ω with $\gamma_m=0.5$ and different ξ_N values. The independence of stability limit upon ξ_N is easily seen and is consistent with the observation from(13).

The simulated displacement responses of free vibration with various Ω values are shown in Fig. 4 where M_N=300kg, $\gamma_m=0.8$, $\omega=2\pi s^{-1}$, $\xi_N=0.2$ and initial condition is d_0=1cm and $v_0=0$. Here ω is fixed while Δt changes to achieve different Ω values. The corresponding $[\Omega]$ is 0.67 obtained with (13). When $\Omega>0.67$, the unstable response is observed in Fig. 4. It is also seen that the simulated result approaches exact one with reducing Ω similar to standard CDM.

B. Dynamic specimen

For the RST of a structure as shown Fig. 2 subject to seismic excitation, $R_E(t)$ is only related to the acceleration a_{EC} (not d_{EC} or v_{EC}) at the coupling degree-of-freedom through following equations.

$$R_{E,i}(t) = -[C_E\, v_{E,i}(t) + K_E\, d_{E,i}(t)] \quad (14)$$

$$M_E\, a_{E,i}(t) + C_E\, v_{E,i}(t) + K_E\, d_{E,i}(t) = -M_E\,(a_{EC,i} + a_{g,i}) \quad (15)$$

in which a_E, v_E, and d_E are the acceleration, velocity, and displacement of experimental substructure relative to the numerical substructure; a_g is the ground acceleration; $t\in[t_{i-1}, t_i]$. Free vibration response of the experimental substructure is obtained using Duhamel's integral on (15). Accordingly, the analytical solution of reaction force is derived. Its substitution together with (6) into (4) gives

$$d_{N,i+1} = c_1\, d_{N,i} + c_2\, d_{N,i-1} + c_3\, d_{N,i-2} + c_4\, d_{E,i} + c_5\, v_{E,i}\, \Delta t \quad (16)$$

in which c_j's are constants related to structural parameters and Δt; their expressions can be found in [7]. Letting

$$\boldsymbol{Y}_{i+1} = \begin{bmatrix} d_{N,i+1} & d_{N,i} & d_{N,i-1} & d_{E,i} & v_{E,i}\Delta t \end{bmatrix}^T \quad (17)$$

one may easily get the corresponding amplification matrix $\boldsymbol{A}$.

It is difficult to obtain the analytical expression of spectral radius of the matrix $\boldsymbol{A}$ due to mathematical complexity. Therefore, the numerical analyses were carried out to investigate the spectral characteristics. Fig. 5a shows the results of undamped cases with frequency ratio γ_ω equal to 1, where $\gamma_\omega = \omega_E/\omega_N$, $\omega_E = \sqrt{K_E/M_E}$, $\omega_N = \sqrt{K_N/M_N}$; the horizontal coordinate is defined as $\Omega=\omega_N\Delta t$. It is seen that $\rho(\boldsymbol{A})$ is always greater than unity, indicating unstable response, however small the mass ratio and Ω are. This means that the CMD is unconditional unstable for a dynamic specimen if there is no damping associated in the test structure. This contrasts the conditional stability of the case with pure inertia specimen and the mass ratio lower than 1. Nonetheless the instability in the case of dynamic specimen is not that serious for small mass ratio and Ω since the spectral radius is very close to unity as shown in Fig. 5a, if only the testing duration is not too long. It is also seen in Fig. 5a that the instability is improved with reduced γ_m, as the spectral radius becomes closer to 1. The elimination of unconditional instability problem can be achieved by adding a damping to the structure. This is illustrated in Fig. 5b where damping ratios of experimental and numerical substructures are both 5%, and $\gamma_\omega=1$. The damping ratio here are defined as $\xi_E=C_E/(2M_E\omega_E)$, and $\xi_N=C_N/(2M_N\omega_N)$. Fig. 6 shows the simulated and exact displacement responses of the free vibrations with $\xi_E=\xi_N=0.05$, $\gamma_m=\gamma_\omega=1$. The initial conditions are: d_{N0}=1cm, d_{E0}=-1cm, $v_{N0}=v_{E0}=0$. Different Ω's are considered in the simulation. The stability limit of this case is 0.44 from Fig. 5b. It is observed from Fig. 6 that the response is unstable when Ω= 0.45, which verifies the result of spectral analysis. Although the stable responses of RST are attained for smaller Ω's, the good agreement with the exact solution is seen only for an Ω as small as 0.05.

IV. NUMERICAL SIMULATION OF RST WITH SHAKING TABLE

In Sections I and II, the dynamics of physical loading system is not considered in order to emphasize the numerical behaviors of the algorithm itself. A shaking table is used in this section as a transfer system of the RST with dynamic specimen, and the stability performance will be investigated through some numerical simulations, in which the linear model of the Rice university shaking table developed by [8] is adopted herein. All the parameters of the shaking table are the same as in [8] except the control gains specified in this paper. The excitation is the El Centro (NS, 1940) earthquake record.

A. Pure Inertia Specimen

The parameters of the numerical substructure and experiment substructures for the numerical simulations are: M_N=300kg, $\omega=2\pi s^{-1}$, $C_N=0$, and $K_E=C_E=0$. Δt =0.01s. The PID control gains are K_P=39.4×5V/m, $K_I=0$, K_D=8.5V·s/m, and the feed-forward and differential pressure control gains are K_{ff}=1.2 V·s/m and $K_{dp}=-2.15\times10^{-7}$V·m^2/N, respectively. The sampling frequency of the digital control is 1000 Hz. The numerical simulation results with different mass ratios and

the exact solution of the displacement responses are shown in Fig. 7. The exact solution is calculated by using LSIM command in Matlab. It is seen that the response becomes unstable when γ_m =1.003. This is consistent with the results of theoretic analysis in Section III. It is also seen that the response approaches the exact solution with smaller γ_m.

B. Dynamic Specimen

The parameters of the numerical substructure, as shown in Fig. 2, are M_N=500kg, ω_N=2πs^{-1}, and ξ_N=0.05. The parameters of the experiment substructure are identical to the numerical substructure, i.e., γ_m=γ_ω=γ_c=1, with γ_C= C_E /C_N. The PID control gains of the shake table controller are: K_P=39.4×5V/m, K_I=0, K_D=7.25V·s/m, and the feed-forward and differential pressure control gains are K_{ff}=1.25 V·s/m and K_{dp}=-2×10^{-7} V·m^2/N, respectively. According the analysis of Section III, the stability limit is equal to 0.44 in this case. The displacement responses of the numerical substructure with different Ω values are shown in Fig. 8. The unstable response is clearly seen when Ω=0.471>[Ω]=0.44. The better result is obtained as expected with smaller Ω.

V. VALIDATION TEST

A validation test was carried out at the Mechanical and Structural Testing Center of the Harbin Institute of Technology. The schematic diagram of the whole test structure is shown in Fig. 1. The experimental substructure was a pure mass made of cast iron with M_E=116kg. A photograph of the experimental substructure installed on the MTS servo-hydraulic actuator is shown in Fig. 9. The circular frequency of the whole structure was kept 2πs^{-1} for all test cases. The damping from the numerical substructure was assumed zero. The integration time interval was 0.01and the sampling frequency was 1024 Hz. Figures 10-12 show the displacement commands and responses of free vibration with different mass ratios. The initial conditions are d_0=0, v_0=3.14cm/s. The stable result was obtained with γ_m=0.1 and the decaying response is observed in Fig. 10, probably due to the friction force between the guiding columns and the iron mass. With this friction force, the response remained stable with γ_m =1.01>1 as seen in Fig. 11. Further increasing γ_m by reducing M_N resulted in an unstable tendency of response as seen in Fig. 12. The test was terminated before it went violently. Although the test results were not exactly the same as predicted by the analytical work in the previous sections, the influence of the specimen mass on the stability of RSTing with the CDM has been confirmed.

It is should be noted that, for pure damping specimen, the stability is reduced by increasing damping level of the specimen [2]. The reason for the different effects of damping could be attributed to by the different damping mechanism of the experimental substructure. The damping in this paper is coulomb-typed friction, while a viscous damping is assumed in [2].

The displacement responses tracked the commands very well in all these cases as shown in Fig. 10-12. The time delay of the displacement responses to the corresponding commands was around 22ms. The focus of this paper was the effects of mass ratio on the stability, and all the test cases were subject to the same time delay, therefore the issues about time delay were not discussed. Nevertheless, the effects of errors such as those due to time delay from testing facilities and relevant improve techniques are apparently important and thus should be investigated further in future study.

It is worth noting that Neild et al. [9] has carried out a similar inertia specimen test using shaking-table as the transfer system and looked at the mass division from control point of view. It was shown there that the division method of the emulated system into the substructure and the numerical model is highly significant to the overall performance of the system.

VI. CONCLUSION

The CDM is modified with an explicit acceleration formulation to obtain correct reaction force of dynamic specimen in a RST. The analytical work, numerical simulation of the RST with a shaking table and actual test have all shown that the stability of the algorithm decreases with increasing mass ratio of experimental over numerical substructures.

VII. APPENDIX: ZERO-STABILITY OF COUPLED CDM

In a hybrid simulation of dynamic system, the solution relies on the two integrations in the time domain: one is numerical and the other is physical. The numerical integration is coupled with physical integration through the interface between the numerical and experimental substructures. A necessary condition for stable solution of the discrete coupled system is zero-stability, i.e., the system is stable as the time integration interval approaches to zero [10]. The objective of this appendix is to confirm the behaviour of the CDM revealed in the third section in this paper, using the method of zero-stability analysis for coupled integration.

For the case of the pure inertia specimen, the outputs of the numerical and experimental substructures at the *i*th step can be expressed as

$$y_{N,i} = a_{N,i-1} \tag{A1}$$

$$y_{E,i} = M_E\, u_{E,i} \tag{A2}$$

and the inputs are related to the outputs by

$$u_{N,i} = y_{E,i} \tag{A3}$$

$$u_{E,i} = y_{N,i} \tag{A4}$$

With (1), and (A1)- (A4) we get

$$\boldsymbol{y}_{i+1} = \boldsymbol{G} + \boldsymbol{H}\,\boldsymbol{y}_i \tag{A5}$$

in which

$$\boldsymbol{G} = \begin{bmatrix} -K_{\mathrm{N}}/M_{\mathrm{N}} & -C_{\mathrm{N}}/M_{\mathrm{N}} \\ -M_{\mathrm{E}}K_{\mathrm{N}}/M_{\mathrm{N}} & -M_{\mathrm{E}}C_{\mathrm{N}}/M_{\mathrm{N}} \end{bmatrix} \boldsymbol{X}_{\mathrm{N},i} \tag{A6}$$

$$\boldsymbol{H} = \begin{bmatrix} 0 & -1/M_{\mathrm{N}} \\ -M_{\mathrm{E}}{}^2/M_{\mathrm{N}} & 0 \end{bmatrix} \tag{A7}$$

$$\boldsymbol{X}_{\mathrm{N},i} = [d_{\mathrm{N},i} \quad v_{\mathrm{N},i}]^{\mathrm{T}}, \text{ and } \quad \boldsymbol{y}_i = [y_{\mathrm{N}.i} \quad y_{\mathrm{E}.i}]^{\mathrm{T}}$$

As it is not difficult to prove that $\boldsymbol{X}_{\mathrm{N},i}$ is a constant for vanishing Δt, $\boldsymbol{G}$ is apparently a constant vector with (A6). Therefore the stability of the system output is determined by $\rho(\boldsymbol{H})$, the spectral radius of $\boldsymbol{H}$. This is easily obtained as

$$\rho(\boldsymbol{H}) = M_{\mathrm{E}}/M_{\mathrm{N}} = \gamma_{\mathrm{m}} \tag{A8}$$

Therefore the output is zero-stable only when

$$\gamma_{\mathrm{m}} \le 1 \tag{A9}$$

This means that any γ_{m} greater than unity will lead to unstable response, which comply with what (13) indicates.

For the case of dynamic specimen, the matrices of $\boldsymbol{G}$ and $\boldsymbol{H}$ are obtained as

$$\boldsymbol{G} = \begin{bmatrix} -K_{\mathrm{N}}/M_{\mathrm{N}} & -C_{\mathrm{N}}/M_{\mathrm{N}} \\ 0 & 0 \end{bmatrix} \boldsymbol{X}_{\mathrm{N},i} + \begin{bmatrix} 0 & 0 \\ -K_{\mathrm{E}} & -C_{\mathrm{E}} \end{bmatrix} \boldsymbol{X}_{\mathrm{E},i+1} \tag{A10}$$

$$\boldsymbol{H} = \begin{bmatrix} 0 & -1/M_{\mathrm{N}} \\ 0 & 0 \end{bmatrix} \tag{A11}$$

For the physical substructure with continuous motion, $\boldsymbol{X}_{\mathrm{E},i+1}$ remains constant for vanishing Δt. Then $\boldsymbol{G}$ is again a constant vector. $\rho(\boldsymbol{H})$ is calculated as zero with (A11), which means that zero-stability is ensured no matter how great γ_{m} is. This matches the result as shown in Fig.5, where $\rho(\boldsymbol{A})$=1 for Ω=0, indicating a stable response.

REFERENCES

[1] M.S. Williams and A. Blakeborough, "Laboratory testing of structures under dynamic loads: an introductory review," Phil. Trans. R. Soc. Lond. A 359, pp. 1651-1669, 2001.

[2] B.Wu, H. Bao, J. Ou, and S. Tian, "Stability and accuracy analysis of central difference method for real-time substructure testing." Earthquake Engineering and Structural Dynamics, 34, pp. 705-718, 2005.

[3] B. Wu, Q. Wang, P.B. Shing, and J. Ou, "Equivalent force control method for generalized real-time substructure testing with implicit integration." Earthquake Engineering and Structural Dynamics, 36, pp. 1127-1149, 2007.

[4] V.T. Nguyen and U. E. Dorka, "Application of digital technique in a control system for real-time sub-structure testing," 4th World Conference on Structural Control and Monitoring, San Diego, USA, 2006.

[5] T. Horiuchi and T. Konno, "A new method for compensating actuator delay in real-time hybrid experiments," Phil. Trans. R. Soc. Lond. A 359, pp. 1893-1909, 2001.

[6] O.S. Bursi, A. Gonzalez-Buelga, L. Vulcan, S.A. Neild, and D.J. Wagg, "Novel coupling rosenbrock-based algorithm for real-time dynamic substructure testing," Earthquake Engineering and Structural Dynamics, 2007, 37, pp. 339-360.

[7] X. Yang, "Numerical simulation of real-time substructure testing with shaking table", Dissertation for the Master Degree Engineering, Harbin Institute of Technology, 2007.

[8] J.P. Conte, and T.L. Trombetti, "Linear dynamic modeling of a uni-axial servo-hydraulic shaking table system," Earthquake Engineering and Structural Dynamics, 2000, 29(9), pp. 1375～1404.

[9] S. A. Neild, D. P. Stoten, D. Drury and D. J. Wagg. "Control issues relating to real-time substructuring experiments using a shaking table," Earthquake Engineering and Structural Dynamics, 2005, 34, pp. 1171 – 1192.

[10] R. Kubler and W. Schiehlen, "two method of simulator coupling." Mathematical and computer modeling of dynamical systems, vol.6 No 2, pp. 93-113, 2000.

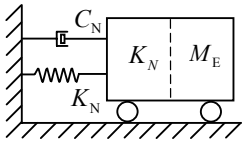

Fig. 1. Computation schematic of structure in RST with pure inertia specimen

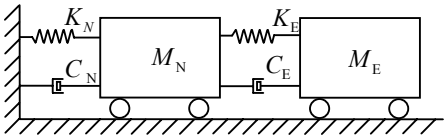

Fig. 2. Computation schematic of structure in RST with dynamic specimen

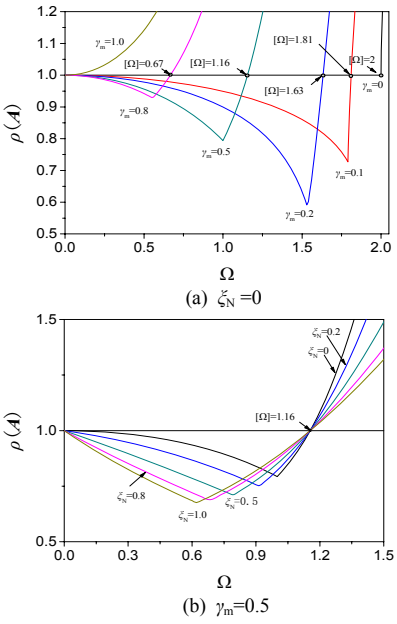

(a) ξ_{N} =0

(b) γ_{m}=0.5

Fig. 3. Spectral radius of CDM for RST with pure inertia specimen

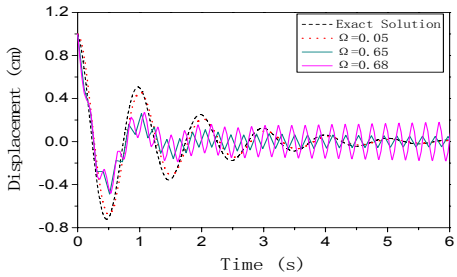

Fig. 4. Free vibration responses with pure inertia specimen

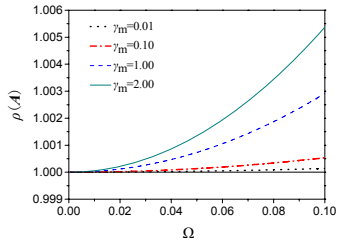

(a) $\xi_N=\xi_E=0$, $\gamma_\omega=1$

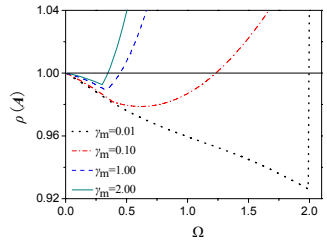

(b) $\xi_N=\xi_E=0.05$, $\gamma_\omega=1$

Fig. 5. Spectral radius of CDM for RST with dynamic specimen

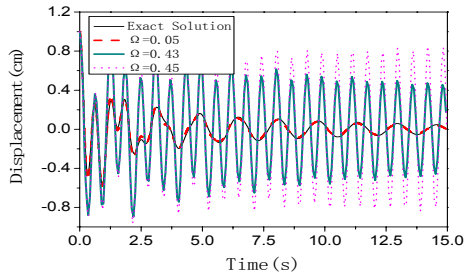

Fig. 6. Free vibration responses with dynamic specimen

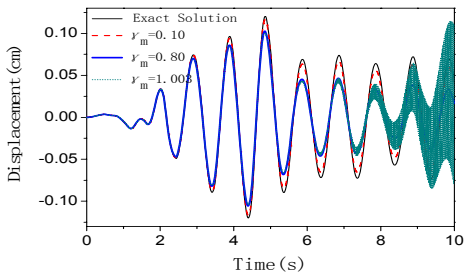

Fig. 7. Numerical Simulation result of RST using shaking table (pure inertia specimen)

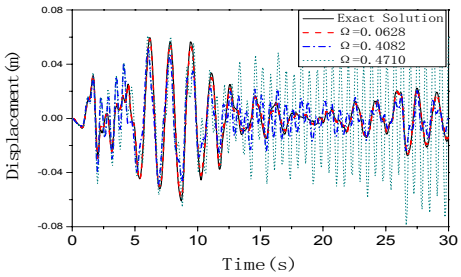

Fig. 8. Numerical Simulation result of RST using shaking table (dynamic specimen)

Fig. 9. Photograph of test setup for RST

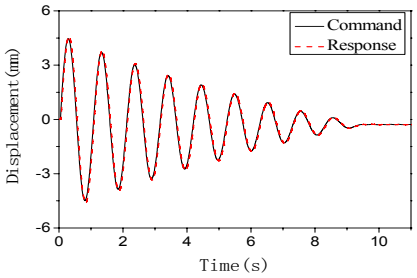

Fig. 10. Test result with $\gamma_m=0.1$

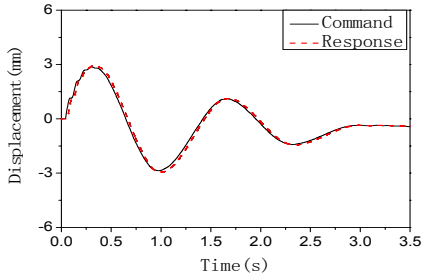

Fig. 11. Test result with $\gamma_m=1.01$

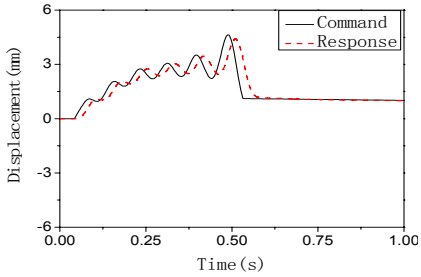

Fig. 12. Test result with $\gamma_m=1.3$